Journal of The Electrochemical Society, **151** (3) F37-F44 (2004) F37
0013-4651/2004/151(3)/F37/8/$7.00 © The Electrochemical Society, Inc.

Organosilicate Spin-on Glasses

I. Effect of Chemical Modification on Mechanical Properties

Suhan Kim,[a] Yvete Toivola,[b] Robert F. Cook,[b,z] Kookheon Char,[a] Sang-Hyun Chu,[c] Jin-Kyu Lee,[d] Do Y. Yoon,[d] and Hee-Woo Rhee[e,*]

[a]*School of Chemical Engineering, Seoul National University, Seoul, Korea*
[b]*Department of Chemical Engineering and Materials Science, University of Minnesota, Minneapolis, Minnesota 55455, USA*
[c]*NIA/NASA Langley Research Center, Hampton, Virginia 23681, USA*
[d]*School of Chemistry, Seoul National University, Seoul, Korea*
[e]*Department of Chemical Engineering, Sogang University, Seoul, Korea*

Methylsilsesquioxane (MSSQ) films were chemically modified by (*i*) the bulk incorporation of a short-chain polymer or (*ii*) surface treatment by an NH_3 plasma, and the effects of these modifications on elastic, plastic, and fracture properties were investigated. In (*i*), a copolymer of 10 mol % 1,2-bis(trimethoxysilyl)ethane (BTMSE) and methyltrimethoxysilane was synthesized and cured to form an MSSQ:BTMSE copolymer film. In (*ii*), an NH_3 plasma treatment was applied to cured MSSQ films for 5, 15, 30, or 60 min. Films were characterized using scanning electron microscopy (SEM), IR spectroscopy, and ellipsometry. Depth-sensing indentation was used to determine plane strain modulus, E', and hardness, H. Indentation traces and SEM images of residual indentation damage were used to determine the threshold load for cracking, P_c. The addition of BTMSE to MSSQ doubled E', H, and P_c relative to MSSQ with a slight increase in relative dielectric constant, k, from 2.70 to 2.86. Apparent E' and H at the surface of plasma-treated films increased with plasma treatment time. IR spectroscopy indicated that improved properties resulted in (*i*) from increased organic and inorganic networking and in (*ii*) from the formation of a dense, largely inorganic, surface layer. Such chemical modifications may be used to improve the performance of organosilicates as low-k dielectrics in microelectronic interconnection structures.
 [DOI: 10.1149/1.1643072]

Manuscript submitted April 7, 2003; revised manuscript received September 11, 2003. Available electronically January 26, 2004.

As feature sizes in microelectronic devices are scaled down, delays in the interconnection array resulting from increased resistance and capacitance coupling (*RC* delay) and ''cross talk'' between metal lines and vias hinders device performance.[1] To improve performance, a change in conductor from aluminum to copper can be made to reduce line resistance and a change in dielectric (insulating) material from silicon dioxide, SiO_2 (dielectric constant, $k = 4$) to a material with lower dielectric constant, low-*k*, can be made to decrease the capacitance between lines and vias.[2]

Many research groups and chemical and semiconductor companies are investigating low-*k* materials suitable for replacing SiO_2. Some candidate replacement materials include nanoporous polyimide ($k \leqslant 2.2$),[3] aromatic thermosetting polymers such as SiLK ($k \approx 2.65$),[4] organosilicates ($k < 3$),[5] and mesoporous silica ($1.8 \leqslant k \leqslant 2.5$).[6] Among these materials, one particularly promising organosilicate low-*k* material is methylsilsesquioxane (MSSQ). It has low dielectric constant ($k \approx 2.7$)[5] and capability for further decreased $k \approx 2.3$ by incorporating nanopores.[7]

A significant challenge facing these groups in developing low-*k* dielectrics for interconnection structures is the maintenance of adequate mechanical properties as the dielectric constant is reduced. During operation, interconnection structures are loaded externally by attachment to the device package and effects of thermal expansion mismatch with the underlying substrate, and internally by line electromigration effects. More severe are the loadings imposed during fabrication from chemical mechanical polishing (CMP), wafer fixturing during film deposition, and dicing.[8] The low-*k* film mechanical properties of interest are the modulus, *E*, hardness, *H*, toughness, *T*, and energy of adhesion to other interconnection materials, *R*. The organosilicate materials are promising in this regard as their SiO_x-based chemistry allows for the possibility of large moduli, hardness and adhesion energies and tunable porosity allow for joint optimization of toughness and dielectric constant.[9]

This paper is Part I of a series and investigates methods for improving the mechanical properties of MSSQ-based materials suitable for low-*k* dielectric applications by two simple types of chemical modification. First, MSSQ is modified by the addition of 10 mol % 1,2-bis(trimethoxysilyl)ethane (BTMSE) monomer to create a copolymer film. The addition of BTMSE, which has greater functionality (number of binding sites) than the base precursor methyltrimethoxysilane (MTMS) and a short carbon chain link between silicon atoms, is intended to enhance network formation and lead to improved mechanical properties. Second, MSSQ films are plasma treated with NH_3 to form modified surface layers.[10] A stiff, dense surface layer could enhance MSSQ film performance during device processing steps such as CMP[11] and packaging, and could also serve as a diffusion barrier between the dielectric and copper lines and vias.[12] The ideas of incorporating short-chain organic monomers to enhance network formation and surface plasma treatments are general ideas which could be used to improve the mechanical properties of other materials in the low-*k* class. In Part II of this series, modification of mechanical properties of MSSQ-based materials by physical means (incorporation of porosity into the MSSQ:BTMSE hybrid) is investigated.

Experimental

Film processing.—Addition of BTMSE to MSSQ as a network modifier.—MSSQ precursors were prepared from MTMS by a procedure described in detail elsewhere.[13] Bridged carbon material, BTMSE, was used as a comonomer by 10 mol % with MTMS to form a MSSQ:BTMSE copolymer, as illustrated Fig. 1.

Silicon (100) wafers were cut into 1×1 cm pieces and cleaned with a piranha solution (H_2SO_4 and H_2O_2, volume ratio 3:1) followed by a deionized water rinse and dried under a nitrogen stream. Solutions of 20 wt % solids (MSSQ or MSSQ:BTMSE) in methyl isobutyl ketone (MIBK) were deposited on the silicon pieces through a syringe with a 0.2 μm polytetrafluroethylene (PTFE) filter and spun cast at 3000 rpm for 30 s. Samples were cured under nitrogen in a curing cycle comprising heating at 3°C/min to 250°C, held at 250°C for 30 min, heated further at 3°C/min to 420°C, and held 40 min (for complete cure) before slow cooling.

* Electrochemical Society Active Member.
z E-mail: rfc@cems.umn.edu

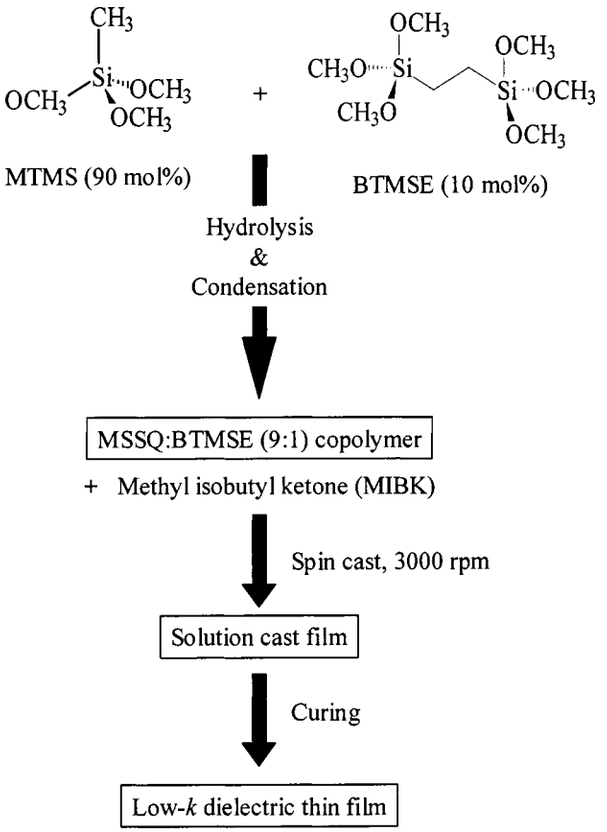

Figure 1. A flowchart showing the procedure used to create base MSSQ and copolymer MSSQ:BTMSE films.

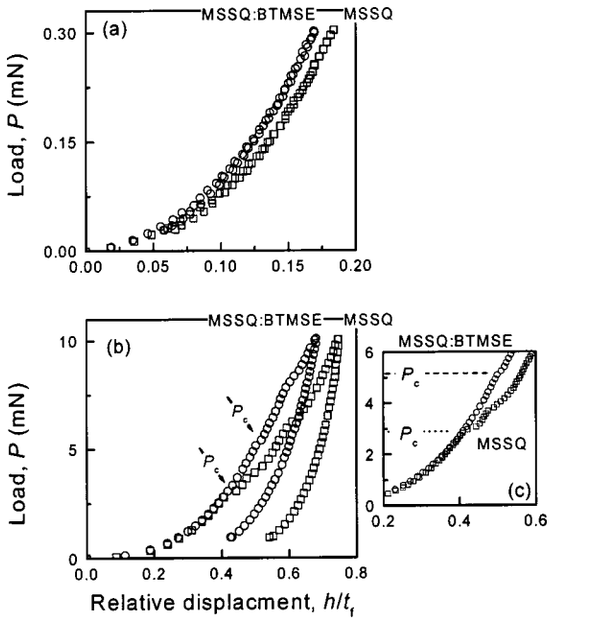

Figure 2. Representative *P*-*h* traces from (a) 0.3 mN peak indentation and (b) 10 mN peak indentation loads in MSSQ and MSSQ:BTMSE films. (c) A magnified plot highlighting the discontinuities associated with film cracking, the crack threshold load, P_c.

NH_3 plasma treatment of MSSQ film.—MSSQ films were treated with NH_3 in a plasma-enhanced chemical vapor deposition (PECVD) system (Surface Technology System 310 C). The flow rate of the treatment gas was fixed at 40 sccm at a pressure of 200 mTorr with radio frequency (rf) power of 60 W. The substrate temperature was held at 300°C during treatment times of 5, 15, 30 or 60 min.

Mechanical and structural characterization.—Depth-sensing indentation (DSI) experiments were performed to determine the apparent plane-strain modulus, E', and hardness, H, as a function of indentation tip displacement, h, using the continuous stiffness measurement (CSM) technique[14,15] (Nanoindenter XP II, MTS Corporation). A Berkovich (three-sided pyramid) diamond tip was used to perform indentations over a peak load range P_{max} = 0.1-300 mN for MSSQ and MSSQ:BTMSE samples. Indentations for plasma-treated samples were performed with the dynamic contact module (DCM) over a peak load range of P_{max} = 0.1-10 mN (MTS Corporation). Indentations performed with the DCM allowed more accurate low-load (surface) measurements to be made.

Modulus and hardness measurements were averaged every 5 nm for four to eight indentations at each peak load on each sample. Additionally, indentation results were used to determine crack threshold load, P_c, and the dissipated energy ratio, $D_{P\text{-}h}$. The crack threshold load for SSQ-based materials has been identified as the first point of discontinuity in the loading slope.[16] The dissipated energy ratio, defined by $D_{P\text{-}h} = (U_{load} - U_{unload})/U_{load}$, is a measure of the relative energy dissipated during contact, where U is the area under the loading and unloading *P*-*h* indentation traces. $D_{P\text{-}h}$ is an objective measure that may be used to gauge changes in contact response, such as the onset of plasticity and fracture events, as a function of indentation tip displacement.

Scanning electron microscopy (SEM) of film-substrate cross sections were used to measure film thickness, t_f, and image changes in films as a function of plasma treatment (JEOL 6500). Film thicknesses were 1.1 and 0.8 μm for MSSQ and MSSQ:BTMSE, respectively. The thickness of all plasma-treated films also fell within this range. Images of the film surface were also used to observe residual indentation damage.

Dielectric and optical characterization.—The dielectric constant, k, of MSSQ and MSSQ:BTMSE copolymer films was measured using metal-insulator-semiconductor (MIS) structures. The addition of BTMSE to MSSQ increased the relative dielectric constant, k, from 2.70 to 2.86. It is believed that the increased k is a result of the greater number of possible nonbridging silanol (Si-OH) groups (six) on the BTMSE monomer relative to that on the MTMS monomer (four). Further increases in k for films with greater BTMSE content than those discussed here support this interpretation.

The refractive index, n, of MSSQ and MSSQ:BTMSE copolymer films was measured using an ellipsometer (L116B-85B, Gaertner sci). (The lack of homogeneity did not allow the refractive index of the plasma-treated films to be measured.) The refractive index of MSSQ was 1.38 ± 0.05 and 1.39 ± 0.05 for the MSSQ:BTMSE copolymer.

Fourier-transform infrared spectroscopy (FTIR) was performed in transmission mode over a frequency range of 4000-400 cm^{-1} with 4 cm^{-1} spectral resolution (Nicolet Series II Magna-IR System 750). Spectra were used to determine chemical species present and quantify peak area changes on chemical modification.

Results

MSSQ and MSSQ:BTMSE copolymer films.—Figure 2a shows DSI traces as a function of relative displacement, h/t_f, for 0.3 mN peak indentation loads in the MSSQ and MSSQ:BTMSE copolymer films. At this low load, peak displacements for both films were less than 20% of the film thickness and contacts for both films were almost elastic (loading and unloading paths are almost coincident). The copolymer film showed smaller displacement at the same load relative to the MSSQ film.

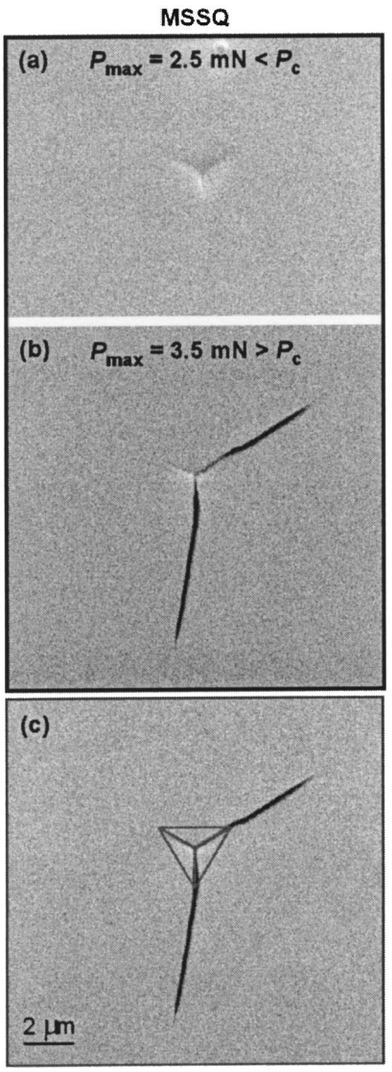

Figure 3. SEM images showing residual damage (cracking and impression) from peak indentation loads (a) just less than (P_{max} = 2.5 mN) and (b) just greater than (P_{max} = 3.5 mN), the crack threshold load, P_c, in MSSQ. (c) The projected contact area at P_{max} = 3.5 mN is drawn to scale over the indentation impression from (b) to highlight film cracking.

Figure 2b shows indentation traces for 10 mN peak loads for the MSSQ and copolymer films; at P_{max} = 10 mN, the peak displacement was near the film-substrate interface for both films. Increased displacements and increased hysteresis were observed in both films relative to their low-load responses of Fig. 2a. Similar to the indentations at lower load, the copolymer film showed smaller peak displacement relative to the MSSQ film. Although the substrate influenced the indentation response, the copolymer film still showed a steeper loading slope (stiffer response) than the MSSQ film.

Discontinuities in the loading slope were also observed for both films in Fig. 2b and are highlighted in Fig. 2c. These discontinuities have been associated previously with film fracture[16] and the first discontinuity has been used to mark the threshold load for cracking, P_c, highlighted in Fig. 2c by a horizontal dashed line. An example is shown in Fig. 3, where SEM images of residual indentation deformation in MSSQ from a peak indentation load of (a) 2.5 mN, slightly less than, P_c, and (b) of 3.5 mN, slightly greater than, P_c. The contact area at peak load was calculated from the contact depth at peak load, $h_c(P_{max})$,[14] from the contact stiffness and displacement at peak load. This contact depth, h_c, was used to calculate the contact radius of an equivalent axisymmetric conical indentation tip (half included angle = 77°) and thus the projected contact area of the Berkovich tip at peak load. Image (c) in the third row is identical to (b) with the Berkovich contact area at peak load drawn to scale over the indentation impression to highlight residual cracking of the MSSQ film.

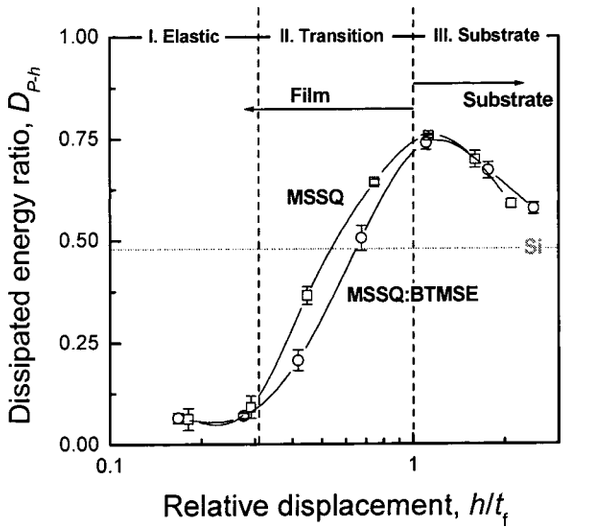

Figure 4. A plot of indentation dissipated energy ratio as a function of relative displacement shows: (I) the films are nearly elastic at low displacements; (II) at moderate displacements, up to the film-substrate interface, the energy dissipated during contact increases due to cracking; and (III) at displacements in which the indenter penetrates the film-substrate interface, the energy dissipated approaches that for the silicon substrate.

Dissipated energy ratio, $D_{P\text{-}h}$, is plotted as a function of relative displacement, h/t_f, in Fig. 4. This plot was divided into three regions denoting changes in behavior from elastic (I), to a transition region (II), to a region where the stiff silicon substrate dominated the indentation response (III). For shallow displacements ($h/t_f < 0.3$), small dissipated energy ratios reflect the largely elastic contact response for both films, illustrated in Fig. 2a. For moderate displacements ($0.3 < h/t_f < 1$), dissipated energy increased with increased displacement, coinciding with the onset of plasticity and film cracking, as illustrated in Fig. 3 and 4. The dissipated energy exhibited a maximum value at the film-substrate interface. For large displacements, ($h/t_f > 1$), the dissipated energy ratio decreased toward the value (~0.48) representative of bulk silicon.

Figure 5 shows apparent plane strain modulus, E', and hardness, H, as a function of relative displacement, h/t_f, measured during a 0.3 mN peak load indentation. Data points below 50 nm are not shown, as the area function used in this analysis is inaccurate at such shallow displacements.[17] It was already shown in Fig. 2a and Fig. 4 that the deformation was mostly elastic for this small load of 0.3 mN. Thus, it is noted that hardness (the mean supported contact stress at peak load), although still meaningful for characterizing indentation contacts, reflects an elastic not plastic response. Figure 5 shows that by the addition of only 10 mol% of BTMSE, E', and H increased by factors of two relative to the base MSSQ material.

Figure 6, summarizing results in Fig. 2-5, shows the increased E', H (at $h/t_f = 0.1$) and P_c of the MSSQ:BTMSE copolymer film relative to the MSSQ film. Adding BTMSE to MSSQ increased the resistance to elastic deformation, plastic deformation, and fracture. This improvement in mechanical properties must result from a structural modification in the copolymer film. Infrared spectroscopy was used to obtain qualitative and quantitative information about the types of bonding modification in the copolymer film relative to MSSQ.

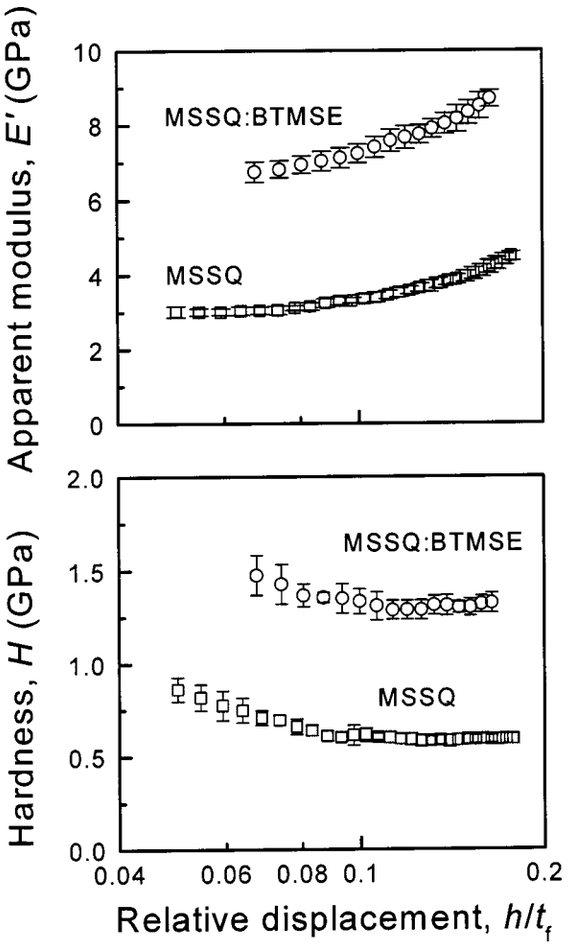

Figure 5. Plots of modulus and hardness as a function of relative displacement for MSSQ and MSSQ:BTMSE films showing increased modulus and hardness for the modified film. The symbols represent the means and standard deviations of four indentation measurements.

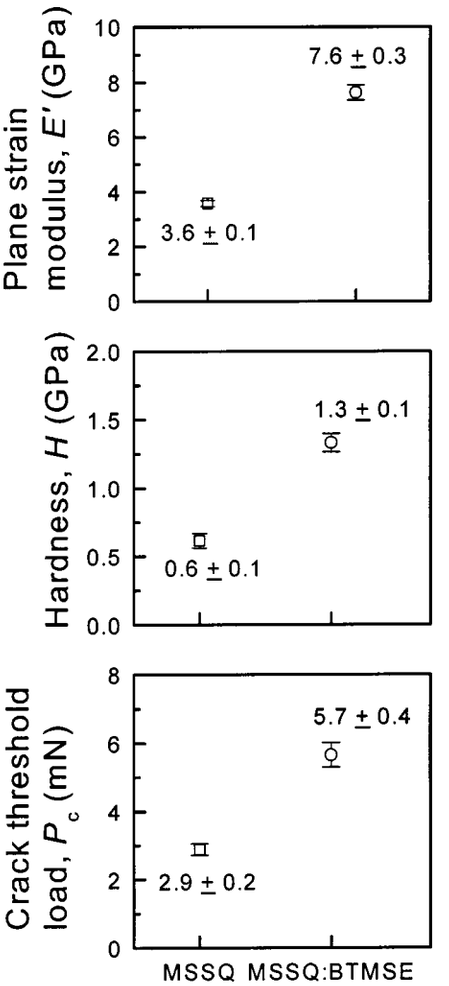

Figure 6. Summary plots showing increased plane strain modulus, E', hardness, H, and cracking threshold, P_c, for the BTMSE:MSSQ copolymer film relative to the unmodified MSSQ film.

IR absorption spectra of MSSQ and MSSQ:BTMSE copolymer films are shown over the full experimental range in Fig. 7a with the MSSQ spectrum indicated as a bold solid line. The overall spectra are quite similar for both films, with main features including CH_3 stretching at 2900 cm^{-1}, symmetric CH_3 deformation (from Si-CH_3) at 1270 cm^{-1}, two discrete O-Si-O asymmetric stretching bands from 1200 to 1000 cm^{-1}, and a band at 780 cm^{-1} from Si-C stretching (and -CH_3 rocking).[18-20]

Spectra were normalized by film thickness and quantitative comparisons were made in specific regions shown in Fig. 7b-d in which differences in the spectra were observed at 1273 and 779 cm^{-1}, corresponding to CH_3 deformations and Si-C stretching, respectively. The decreased peak intensity at 1273 and 779 cm^{-1} shown in Fig. 7b-c corresponded to the decreased number of methyl (-CH_3) groups due to BTMSE substitution for 10 mol % MTMS. The CH_3 deformation band of MSSQ:BTMSE decreased in area by 13.3% relative to that of MSSQ. Changes in the Si-C stretching band were not quantified as it overlaps with the Si-O bending vibration. Figure 7c also shows the appearance of a small shoulder in the MSSQ:BTMSE spectrum near 730 cm^{-1}, corresponding to the CH_2-CH_2 rocking vibration.[18] The appearance of this vibration confirmed the presence of bridged carbon chains (Fig. 1) in the MSSQ:BTMSE film after curing.

Finally, changes in the O-Si-O stretch from 1200 to 1000 cm^{-1} are shown in Fig. 7d and a spectrum from a PECVD SiO_2 film is also included for comparison. MSSQ films in this study were synthesized from MTMS, which forms an MSSQ network through the condensation reaction shown at the top of Fig. 8a. This condensation reaction joins siloxanes through -OH groups to create a single O-Si-O bond[13] and continues to proceed to an extent dependent on the curing time and temperature, such that various derivatives of condensed species may exist after curing. For complete condensation up to three O-Si-O bonds are formed and four O-Si-O bonds are created only when a terminal -CH_3 group is lost.

Wang *et al.*[19,20] have suggested deconvolution of the O-Si-O band with four Gaussian peaks. In this paper, a similar approach was taken and the molecular species attributed to the four peaks within the O-Si-O band are shown in the schematic structure of a partially condensed MSSQ structure of Fig. 8a and listed in Table I. The species are assigned as M, D, Q, and T in order from the highest to the lowest vibration frequency where M stands for silicon with one O-Si-O bond, D is for silicon with two O-Si-O bonds, T is for silicon with three O-Si-O bonds (siloxane trimer[18]), and Q is silicon fourfold coordinated with oxygen (as in SiO_2). Previously published IR results[19,20] have shown that for high-temperature curing (T_{cure} $> 500°C$) of MSSQ in air, the number of -CH_3 groups decreases and there is a corresponding peak shift in the O-Si-O vibration from 1030 (T) to 1070 cm^{-1} (Q), the dominant O-Si-O peak at 1080 cm^{-1} for PECVD SiO_2, as shown in Fig. 7d.

Absorption from D and T structures accounted for the majority of the O-Si-O band for MSSQ; Q absorption was relatively broad

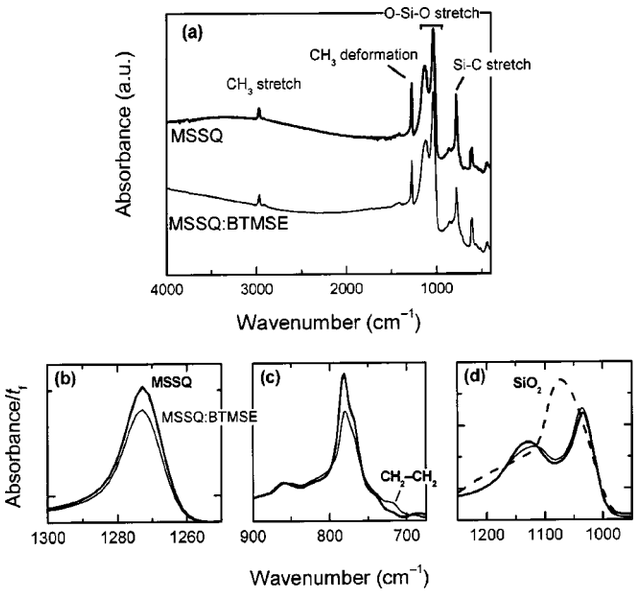

Figure 7. (a) IR spectra for MSSQ and MSSQ:BTMSE films. (b) The CH_3 deformation band of MSSQ:BTMSE decreased in area by 13.3% relative to that of MSSQ. (c) CH_2-CH_2 vibrations, confirming the presence of BTMSE bridging elements in the MSSQ:BTMSE copolymer film after curing. (d) The O-Si-O stretching peaks shown as absorbance normalized by film thickness, indicating increased networking and modified cage structures for the copolymer film.

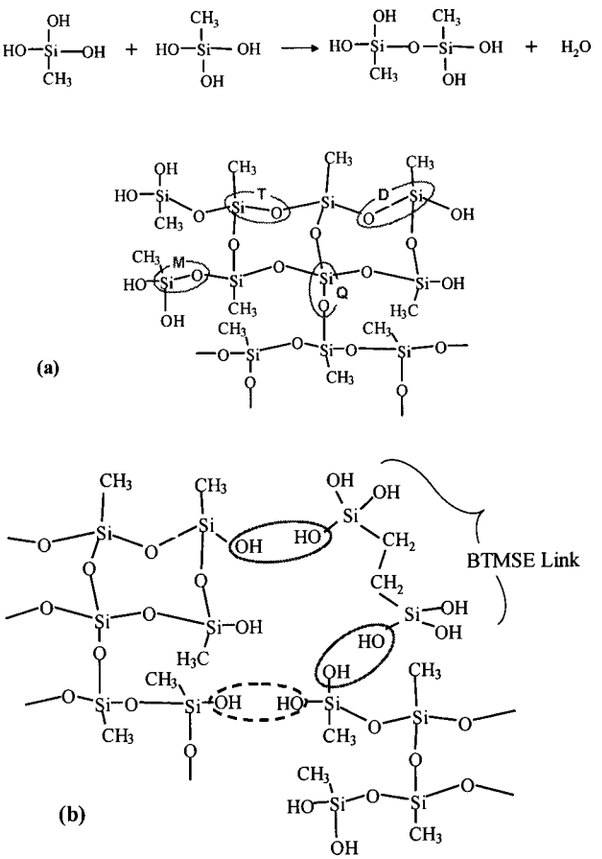

Figure 8. 2D schematic representations of (a) a partially condensed MSSQ structure, indicating the IR peak assignments, and (b) two partially condensed MSSQ structures linked by a single BTMSE monomer.

and low intensity, and M contributed very little to the vibration band. The MSSQ:BTMSE film showed an increased number of T species. D absorption shifted to a higher energy vibration along with the appearance of a shoulder on the high-frequency vibration end (as though it had split into two peaks). The peak shift may result from the formation of -O-Si-CH_2-bonds when a BTMSE monomer links partially condensed MSSQ structures, as outlined in Fig. 8b by a solid border. BTMSE can bind up to six partially condensed MSSQ structures, thereby enhancing the connectivity within the copolymer film. In addition, the flexibility of the carbon backbone can enhance film networking by bringing in close proximity two partially condensed MSSQ structures. They may then be able to form a bond by the condensation reaction of their terminal -OH groups, thus forming an O-Si-O bond as outlined in Fig. 8b by a dashed border.

It has been explained in a previous publication[13] that the reaction conditions (time, temperature, humidity, and so on) can change the final structure of a film, and it is noted here that different reaction conditions existed for the MSSQ film and the MSSQ:BTMSE copolymer film, principally the reaction time. Reaction times for conversion from MTMS to MSSQ are on the order of 12 h, while the reaction time for the mixture of MTMS and BTMSE was on the order of 6 h. Consequently, the observed increase in networking is attributed to the addition of BTMSE and not to the difference in reaction conditions.

Plasma-treated MSSQ films.—Figure 9 shows SEM images of cross-sectioned films on silicon for untreated MSSQ and films plasma treated for 5 and 15 min. From these images it can be seen clearly that a discrete surface layer 120-140 nm thick was formed for the 5 and 15 min plasma-treated films. Base MSSQ samples and films plasma treated for 30 and 60 min did not show this discrete surface layer.

Figure 10a shows indentation *P-h* traces for 0.3 mN peak load indentations in untreated (solid line) and 5 and 60 min plasma-treated (open symbols) MSSQ films. For 0.3 mN peak loads, displacements at peak load penetrated the plasma-modified surface layer and reached a peak depth of almost 200 nm. All films showed very little hysteresis for these shallow indentations. Untreated MSSQ showed the largest displacement, and the film plasma treated for 60 min showed the least displacement at a given load. Although the *P-h* responses of the 15 and 30 min plasma-treated films are not shown (for clarity), it is noted that there was no systematic correlation between plasma treatment time and displacement at peak load.

Figure 10b shows *P-h* traces for 10 mN peak load indentations in untreated and 5 and 60 min plasma-treated MSSQ films. At this load, peak displacements nearly reached the film-substrate interface. All plasma-treated films showed similar *P-h* behavior and all showed smaller peak displacements relative to the untreated MSSQ film. There was increased hysteresis relative to the traces shown in Fig. 10a and discontinuities in the loading slope were apparent.

SEM images in Fig. 11 show the residual damage from 10 mN peak indentation loads on the surface of the untreated MSSQ film and the films treated for 5 and 60 min. On the right of each image an outline of the contact area at peak load is superimposed to highlight cracking. From these images it is clear that the untreated MSSQ film had longer radial cracks than either of the plasma-treated films. The residual cracks for both plasma-treated films look very similar.

Table I. IR peaks and their assignments for O-Si-O stretch of MSSQ and SiO_2.

Peak	MSSQ	SiO_2	Assignments
T	1033 (cm^{-1})		O-Si-O with terminal -CH_3
Q	1070 (cm^{-1})	1087 (cm^{-1})	O-Si-O, SiO_2-like
D	1127 (cm^{-1})		O-Si-$(OH)_2$ with terminal -CH_3
M	1209 (cm^{-1})		O-Si-$(OH)_3$ with terminal -CH_3

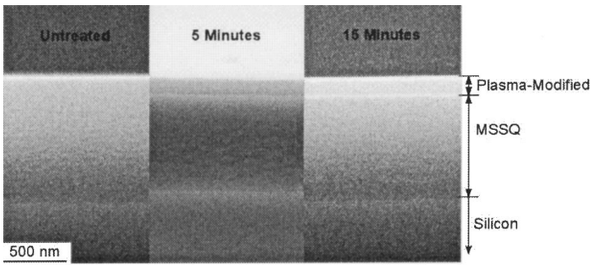

Figure 9. An SEM image showing the cross sections of MSSQ films on a silicon substrate after 5 and 15 min of plasma treatment. Both images show that a discrete surface layer was formed with a thickness of ~100 nm.

There is a faint residual impression correlated with the indentation contact outline at peak load in the film treated for 5 min that is not visible in the film treated for 60 min.

Figure 12 shows the apparent plane strain modulus, E', and hardness, H, measured as a function of depth during a 0.3 mN peak load indentation of untreated and plasma-treated MSSQ films. Plasma-treated films are shown as open symbols and untreated MSSQ is shown as a solid line. Data points at displacements less than 50 nm are shown for relative comparison and are not representative of absolute modulus and hardness values at those shallow displacements. Both the uncertainty in tip shape and the inhomogeneous film properties make it impossible to determine the actual modulus or hardness using this experimental technique over this depth range. However, the untreated MSSQ film modulus and hardness remain almost invariant for shallow displacements, h, ranging from 12 nm (where the tip area function is inaccurate) to 80 nm. Therefore, the relatively large increase in apparent modulus and hardness with plasma treatment at shallow displacements ($h < 50$ nm) are not attributed to tip shape error.

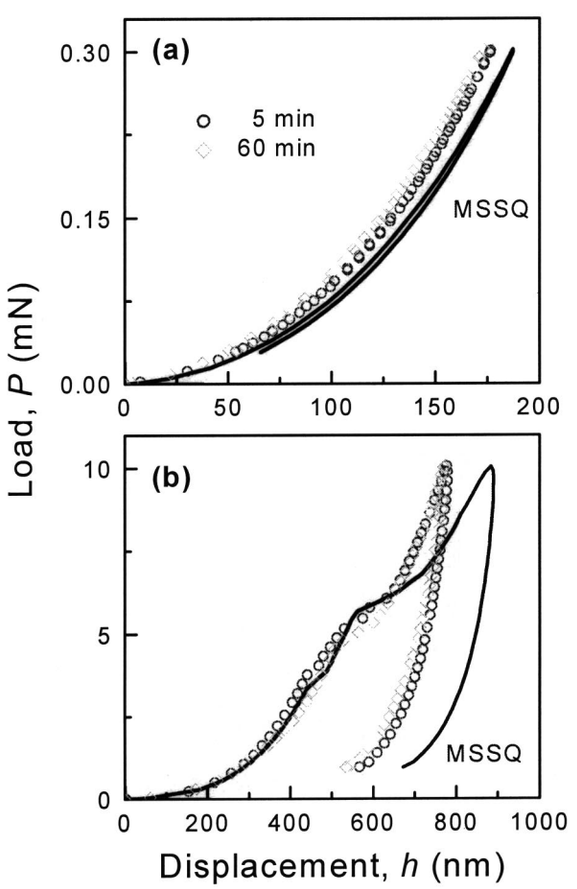

Figure 10. Representative P-h traces from (a) 0.3 mN indentation and (b) 10 mN indentation loads for untreated and 5 and 60 min plasma-treated MSSQ films. The P-h trace of untreated MSSQ is shown as a solid line.

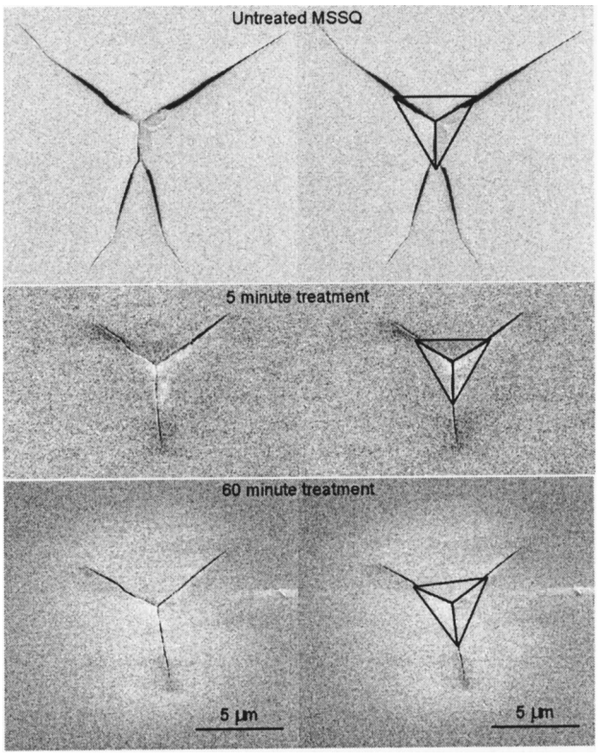

Figure 11. A set of SEM images showing residual deformation (cracking and residual impression) from 10 mN indentations in untreated, 5, and 60 min plasma-treated films.

At a shallow displacement of 12 nm it is shown that the apparent moduli of all plasma-treated films were greater than that of the untreated MSSQ film and also increased with increased plasma treatment time. While the modulus for the untreated MSSQ film remained almost constant from 12 to 80 nm of displacement, the apparent moduli of all plasma-treated films decreased with increased displacement. From the SEM images in Fig. 9 it was clear that the discrete surface layer thickness was ~120 nm. The apparent modulus decrease with the increase in displacement for depths less than 100 nm is a result of the increased influence of the relatively compliant MSSQ sublayer.

Changes in apparent modulus were not linear with plasma treatment time. There was a relatively large increase in modulus from the value for the untreated film after only 5 min of plasma treatment. Relatively smaller increases in apparent modulus were seen for 15 and 30 min of treatment relative to the increase after only 5 min. There was another relatively large increase in apparent modulus observed for the film plasma treated for 60 min relative to all other plasma treatment times.

At a displacement of 100 nm ($h/t_f \approx 0.1$), all plasma-treated films had an apparent modulus greater than that of the untreated MSSQ film. Films that were plasma treated for 5, 15, and 30 min collapse to a single value while the film treated for 60 min remained at an increased apparent modulus. The increase in apparent modulus at this displacement may result from inadvertent film modification during plasma treatment. The substrate temperature was held at 300°C during plasma treatment and during the plasma treatment times of 30 and 60 min the film is subjected to this temperature for a period of time comparable to curing. For short plasma treatment

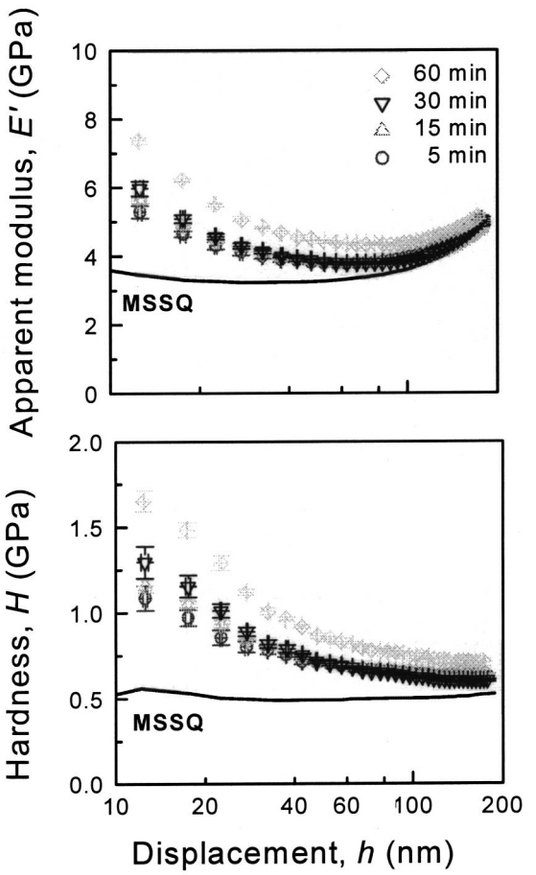

Figure 12. Plots of modulus and hardness as a function of relative displacement for untreated and plasma-treated MSSQ films.

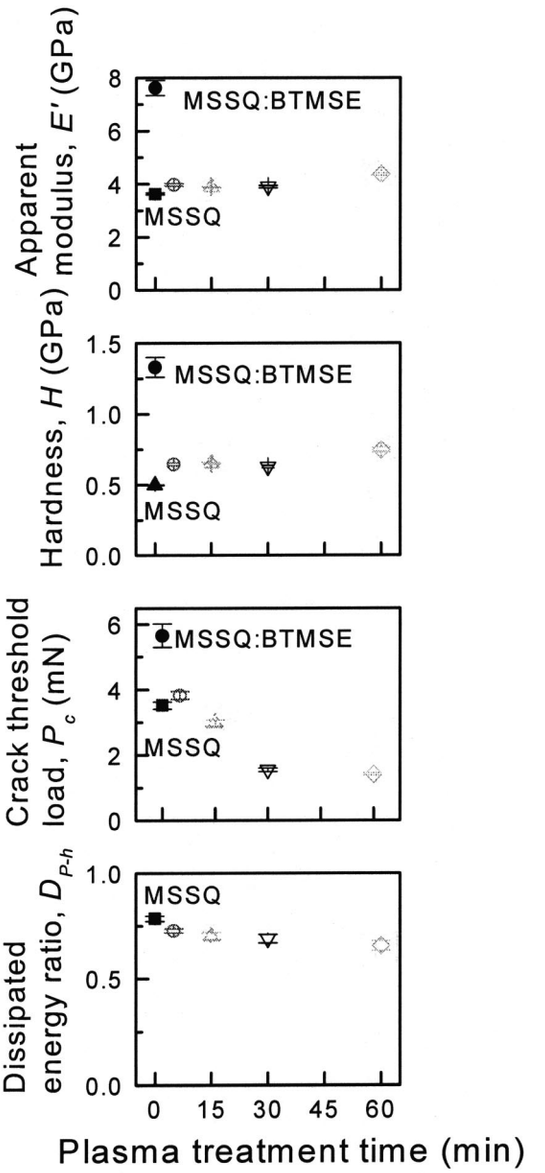

Figure 13. Summary plot of E_f', H ($h = 100$ nm), P_c, and $D_{P\text{-}h}$ (from a 10 mN peak load) as a function of plasma treatment time showing the effect of plasma treatment on MSSQ films relative to untreated MSSQ and MSSQ:BTMSE films.

times of 5 and 15 min, SEM images showed that a modified surface layer ~120 nm thick was formed. For longer plasma treatment times, this modified surface layer must have formed after a short time (~5 min). However, it is possible that the MSSQ sublayer may have been modified (*i.e.*, further cured) as a result of the elevated substrate temperature during plasma treatment.

Hardness is shown as a function of displacement in Fig. 12. The hardness of the untreated MSSQ film was almost constant from 12 nm of displacement to almost 200 nm. At any depth, it can be seen that the hardness of all plasma-treated films was greater than that of the untreated film. Hardness of the plasma-treated films was greatest at the shallowest depth shown (~12 nm) and decreased with increased displacement. This may be anticipated as the plasma treatment is expected to be mainly a surface modification. Similar to results discussed for the apparent modulus, all plasma-treated films converged to a single hardness value at a displacement of ~100 nm, except for the film treated for 60 min. This supports the possibility of additional chemical or structural modifications occurring below the plasma-treated surface layer as a result of long plasma treatment time at an elevated temperature.

Figure 13 is a plot summarizing changes in the plane strain modulus, E', hardness, H, ($h = 100$ nm), crack threshold load, P_c, and dissipated energy ratio, $D_{P\text{-}h}$, as a function of plasma treatment time, measured from the 10 mN peak indentation load. MSSQ and MSSQ:BTMSE are shown at time 0 for comparison. E' and H increased after 5 min of plasma treatment and remained almost constant through 30 min of plasma treatment and increased for 60 min plasma treatment. For a 5 min plasma treatment, P_c increased slightly relative to the untreated film and then decreased slightly with increased plasma treatment time. $D_{P\text{-}h}$ decreased as a function of increased plasma treatment time. One may anticipate this sort of decrease in dissipated energy as modulus and hardness increased with increased plasma treatment time and the edges of the indenter remained in contact with the surface-modified layer, although the tip penetrated to a peak depth of ~800 nm.

The entire IR spectra of untreated and plasma-treated MSSQ films are shown in Fig. 14a. The spectra look very similar, as the chemical modifications by plasma treatment might be expected predominantly at the surface (*i.e.*, top 100 nm) of the films. Ammonia plasma treatments have been demonstrated previously to form silicon nitride at the surface of other SiO_x-based films.[10,21,22] Figure 14b shows similar evidence as a shoulder developed with increased plasma treatment time near the Si-N-Si stretching vibration at 900 cm^{-1}. There were neither obvious changes in $-CH_3$ content nor the evidence of remnant ammonia species. The four-peak deconvolution of the O-Si-O band showed no systematic change in the number of M, D, or T species with plasma treatment time. However, the num-

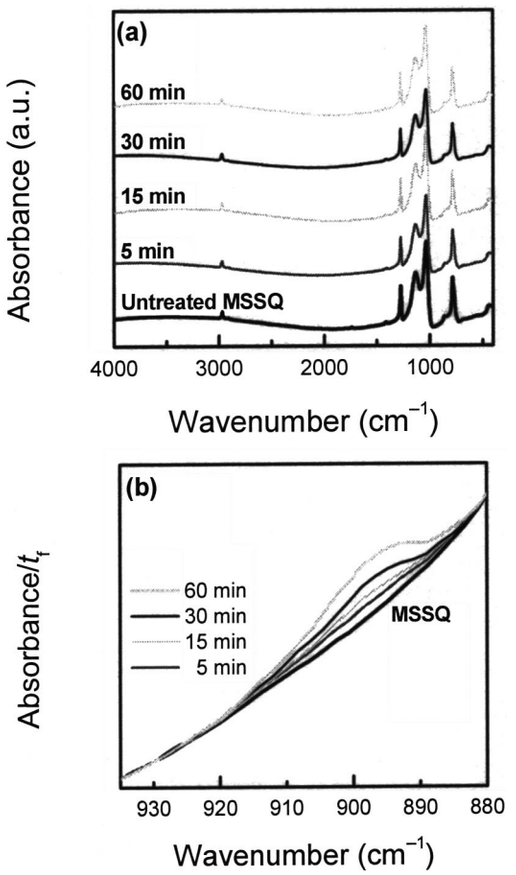

Figure 14. (a) IR spectra for untreated and plasma-treated MSSQ films. (b) The appearance of a shoulder corresponding to the N-Si-N stretch developed at 900 cm^{-1} with increased plasma treatment time.

ber of Q species did increase systematically with plasma treatment time, similar to results shown for NH_3 plasma treatment of other SiO_x-based films.[10,21]

Conclusion

Two different chemical modifications were shown to improve the mechanical properties of conventional organosilicate MSSQ films. First, a chemical modification of the entire film was achieved by the addition of BTMSE. The MSSQ:BTMSE (9:1 mol %) copolymer film exhibited modulus and hardness values a factor of two greater than that of MSSQ. The threshold load for indentation fracture was also increased in the copolymer film and shorter indentation cracks were observed in the copolymer film relative to those in the MSSQ film for indentation loads greater than the threshold. Infrared spectroscopy revealed both increased O-Si-O networking and the existence of CH_2-CH_2 bridges for the copolymer film after curing, suggesting that the improved mechanical properties of the copolymer derived from both increased inorganic and organic bridging. The changed nature of the bridging (and perhaps an increase in the number of nonbridging Si-OH) groups led to a small increase in dielectric constant of approximately 6%.

Second, a chemical modification of the surface of MSSQ films was achieved by an NH_3 plasma treatment. The formation of a modified surface layer was confirmed using cross-sectional SEM. Infrared spectroscopy indicated the formation of SiN_x and the systematic increase in the number of Q or SiO_2-like species with increased plasma treatment time. The films exhibited increased apparent modulus and hardness values after just 5 min of plasma treatment, with the surface of the film showing the greatest increases, which further increased with increasing plasma treatment. It is suggested that the formation of a predominantly inorganic, denser structure in the surface lead to the improved elastic and plastic properties on plasma treatment.

Interpretation of crack initiation loads (which decreased with increasing treatment time) was complicated by the geometric structure of the plasma-treated films: a stiff surface layer, on a relatively compliant sublayer, on a stiff silicon substrate. However, SEM images of residual indentation damage showed shorter radial cracks in plasma-treated MSSQ films relative to the untreated MSSQ film. For a stiff layer on a relatively compliant substrate, the underlying substrate carries the majority of the deformation.[23] Therefore, for the film plasma treated for 5 min, the discrete stiff surface layer may have deformed as a blanket film while the relatively compliant, unmodified SSQ sublayer accommodated the majority of the deformation until cracking occurred. For the longer plasma treatment times, where no discrete layer was observed, the distribution of stress during indentation may have been more evenly distributed through the thickness of the film, changing the character of the indentation damage and hence the relative meaning of cracking threshold.

Acknowledgments

This work is supported by the Korean Collaborative Project for Excellence in Basic System IC Technology (System IC 2010: 98-B4-C0-00-01-00-02). Financial support from the Ministry of Science and Technology (MOST) and the Korean Ministry of Education through the National Research Laboratory Fund and the Brain Korea 21 Program, respectively, is also greatly acknowledged.

The University of Minnesota assisted in meeting the publication costs of this article.

References

1. *The International Technology Roadmap for Semiconductors*, Semiconductor Industry Association, San Jose, CA (2002).
2. P. Singer, *Semicond. Int.*, **20**, 67 (1997).
3. J. L. Hedrick, R. D. Miller, C. J. Hawker, K. R. Carter, W. Volksen, D. Y. Yoon, and M. Trollsås, *Adv. Mater. (Weinheim, Ger.)*, **10**, 1049 (1998).
4. S. J. Martin, J. P. Godschalx, M. E. Mills, E. O. Shaffer II, and P. H. Townsend, *Adv. Mater. (Weinheim, Ger.)*, **12**, 1769 (2000).
5. S. M. Kim, D. Y. Yoon, C. V. Nguyen, J. Han, and R. L. Jaffe, *Mater. Res. Soc. Symp. Proc.*, **511**, 39 (1998).
6. S. Baskaran, J. Liu, K. Domansky, N. Kohler, X. H. Li, C. Coyle, G. E. Fryxell, S. Thevuthasan, and R. E. Williford, *Adv. Mater. (Weinheim, Ger.)*, **12**, 291 (2000).
7. A. T. Kohl, R. Mimna, R. Shick, L. Rhodes, Z. L. Wang, and P. A. Kohl, *Electrochem. Solid-State Lett.*, **2**, 77 (1999).
8. G. W. Ray, *Mater. Res. Soc. Symp. Proc.*, **511**, 199 (1998).
9. R. F. Cook, *Mater. Res. Soc. Symp. Proc.*, **576**, 301 (1999).
10. K.-M. Chang, I.-C. Deng, S.-J. Yeh, and Y.-P. Tsai, *J. Electrochem. Soc.*, **147**, 1957 (2000).
11. M. K. Jain, G. A. Dixit, M. F. Chisholm, T. R. Seha, K. J. Taylor, G. B. Shinn, and R. H. Havemann, *Proc. SPIE*, **2335**, 2 (1994).
12. K.-M. Chang, I.-C. Deng, S.-J. Yeh, and Y.-P. Tsai, *Electrochem. Solid-State Lett.*, **2**, 634 (1999).
13. J.-K. Lee, K. Char, H.-W. Rhee, H. W. Ro, D. Y. Yoo, and D. Y. Yoon, *Polymer*, **42**, 9085 (2001).
14. W. C. Oliver and G. M. Pharr, *J. Mater. Res.*, **7**, 1564 (1992).
15. J. B. Pethica and W. C. Oliver, *Mater. Res. Soc. Symp. Proc.*, **130**, 13 (1989).
16. Y. Toivola, J. Thurn, and R. F. Cook, *J. Electrochem. Soc.*, **149**, F9 (2002).
17. J. Thurn and R. F. Cook, *J. Mater. Res.*, **17**, 1143 (2002).
18. G. Socrates, *Infrared and Raman Characteristic Group Frequencies: Tables and Charts*, John Wiley & Sons, Inc., New York (2001).
19. C. Y. Wang, Z. X. Shen, and J. Z. Zheng, *Appl. Spectrosc.*, **54**, 209 (2000).
20. C. Y. Wang, Z. X. Shen, and J. Z. Zheng, *Appl. Spectrosc.*, **55**, 1347 (2001).
21. T. C. Chang, Y. S. Mor, P. T. Liu, T. M. Tsai, C. W. Chen, Y. J. Mei, and S. M. Sze, *Thin Solid Films*, **398-399**, 632 (2001).
22. P.-T. Liu, T.-C. Chang, Y.-L. Yang, Y.-F. Cheng, and S. M. Sze, *IEEE Trans. Electron Devices*, **47**, 1733 (2000).
23. T. Y. Tsui, J. Vlassak, and W. D. Nix, *J. Mater. Res.*, **14**, 2204 (1999).